COMPARISON OF VENTRICULAR GEOMETRY FOR TWO REAL TIME 3D ULTRASOUND MACHINES WITH THREE DIMENSIONAL LEVEL SET

E. Angelini, R. Otsuka, S. Homma, A. Laine

Columbia University, New York, USA

ABSTRACT

This paper presents new results for segmentation of 3D ultrasound using a robust and smooth segmentation method based on a homogeneity-driven three dimensional level set algorithm. The segmentation was applied to echocardiographic data from healthy volunteers acquired with two 3D ultrasound machines based on matrix-phased array technology. A comparison of ventricular volumes and geometry is performed based on manual and automatic methods of segmentation. Results showed good agreement of the segmentation methods and the ultrasound machines for ventricular geometry and quantitative assessment of cardiac function.

1. INTRODUCTION

Segmentation of three-dimensional ultrasound data is gaining more interest along with constant improvement in image quality. The challenge of developing a segmentation tool for quantification of cardiac function from three-dimensional ultrasound lies in the wealth of dynamic information that can be extracted despite its relatively low spatial resolution and high level of speckle noise. We have been specifically interested in the use of real-time three-dimensional ultrasound data acquired with matrix-phased array transducers [1]. The poor quality of the ultrasound signal has limited the acceptance of 3D ultrasound technology in clinical practice, despite the wealth of information acquired by such systems, far greater than with any other existing echocardiography screening modality. The work presented in this paper aimed to improve the better acceptance of this new technology by addressing the problem of automatic quantification of ventricular function. We were especially interested in comparing the performance of two ultrasound machines: Volumetrics (no longer marketed) and the new Sonos 7500 machine from Philips Medical Systems. Both machine are available in the Echocardiography Laboratories at Columbia University and were used in this study to screen healthy volunteers.

The segmentation method developed in this work is based on implicit deformable models implemented within a level set framework [2]. Level set segmentation methods have been applied to a wide range of medical screening modalities for anatomical volume segmentation, shape representation and deformation modelization as reviewed in [3-5]. The energy functional controlling the deformations is derived from the approach recently proposed by Chan and Vese [6] inspired by the homogeneity-based Mumford-Shah segmentation technique [7]. Homogeneity-based methods are best suited for 3D ultrasound images where the myocardium wall is depicted as a bright textured object without well defined borders.

2. METHOD

2.1. Mumford-Shah Level set functional

Our segmentation algorithm is derived from the Mumford-Shah functional [6] using the energy functional proposed in [6]. The segmentation of a volume data *I* is performed via deformation of an initial curve *C* to minimize the following energy functional:

$$E(C,c_0,c_1) = \mu L(C) + \nu A(C) + \lambda_0 \int_{inside(C)} |I_0 - c_0|^2 \, d\Omega + \lambda_1 \int_{outside(C)} |I_0 - c_1|^2 \, d\Omega \quad (1)$$

where c_0 and c_1 are equal to the average of the volume data *I* inside and outside of the curve C, $L(C)$ is the length of the curve and $A(C)$ the area of the curve.

2.2. Level set implementation

Energy minimization of Equation (1) was performed with the level set framework introduced by Osher and Sethian [8]. To use such level set framework, the curve C is embedded in a Lipschitz scalar function ϕ defined on $\mathbb{R}^N$, such that:

$$\begin{aligned} C &= \{x \in \mathbb{R}^N / \phi(x) = 0\}, \\ C_{inside} &= \{x \in \mathbb{R}^N / \phi(x) < 0\}, \\ C_{outside} &= \{x \in \mathbb{R}^N / \phi(x) > 0\}. \end{aligned} \quad (2)$$

The level set implementation of the energy functional replaces the n-D curve C by an n+1-D function ϕ and solves the minimization problem for the energy functional reformulated with the level set function as:

$$E(\phi, c_0, c_1) = \mu L(\phi = 0) + \nu A(\phi \le 0) + \lambda_0 \int_\Omega |I - c_0|^2 H(\phi)\, d\Omega + \lambda_1 \int_\Omega |I - c_1|^2 (1 - H(\phi))\, d\Omega \quad (3)$$

To rewrite the functional of Equation (1) as a function of ϕ, two mathematical functions were used to define the interior and the contour of the curve C:

(1) a Heaviside function: $H(z) = \begin{cases} 1 \text{ if } z \le 0 \\ 0 \text{ if } z \ge 0 \end{cases}$, (4)

(2) a Dirac function: $\delta(z) = \frac{dH(z)}{dz}$. (5)

The use of these two functions enables us to rewrite the regularization terms $L(C)$ and $A(C)$ in terms of integrals over the entire data domain. With this level set framework, the final solution C_0 to the initial minimization problem corresponds to the zero-level of the final solution ϕ_0 of the level set framework energy functional.

2.3. Dynamic Implementation

Computation of the Euler-Lagrange equation associated with the minimization of Equation (3) requires regularization of the Heaviside and Dirac functions [6, 9]. In our implementation, we have chosen the regularization functions $H_\varepsilon(\phi)$ and $\delta_\varepsilon(\phi)$ proposed by Chan et al. in [6] with $\varepsilon = 2$. The Euler-Lagrange equation, as derived in [6], is therefore expressed as:

$$\delta_\varepsilon(\phi)\left[\mu\, div\left(\frac{\nabla\phi}{|\nabla\phi|}\right) - \nu - \lambda_0 (I - c_0)^2 + \lambda_1 (I - c_1)^2\right] = 0 \quad (6)$$

We observe here the introduction of the curvature of the zero-level front $K(\phi) = -div\left(\frac{\nabla\phi}{|\nabla\phi|}\right)$, as with the popular level set algorithm for segmentation via motion under mean curvature introduced by Osher and Sethian [8].

2.4. Discretization and Parameters Values

Implementation was performed with a finite difference scheme for spatial derivatives and the introduction of an artificial time component to model the descent iteration. The curvature term [6] was computed with a scheme initially proposed by Rudin, Osher and Fatemi in [10], which combined both centered and one-sided spatial derivatives but did not explicitly include cross derivatives. Chan and Vese also used an implicit scheme for the curvature term to constrain the bounds of ϕ^n and ϕ^{n+1} to be similar [11] and make the numerical scheme unconditionally stable. Unconditional stability allows for arbitrary time step values to speed up the iteration process. An initial implementation of the algorithm for segmentation of RT3D ultrasound used an explicit scheme for the time derivative [12]. Such implementation constrains the time step used for the iterative optimization to be limited by the CFL condition. We observed that this narrowed the flexibility of the algorithm and our ability to use all parameters to finely control the behavior of the deforming front.

There are four parameters for the energy functional associated with the homogeneity terms and the regularizing terms: $(\lambda_0, \lambda_1, \mu, \nu)$. Setting these parameters is a very delicate task that was carried out via an experimental approach. Final values were set as follows: $\upsilon =$ -0.00003 $\times \text{size}(\text{Volume})$ with a negative sign to force the surface to expand, $\mu =$ -.00003 $\times \left(1/\text{Maxi\_diagonal\_distance}\right) \times size(Volume)$ with a negative sign to force the surface to have minimal length, $\lambda_1 = \lambda_2 = 100$. As we can see here, the two regularizing terms were used to enforce some smoothness of the final surface to enclose a maximum volume with a minimal surface area. We also observed the dependence of these terms to the data size, as suggested by Chan and Vese. For the homogeneity terms, the same importance was given to the inside blood cavity and the outside myocardial tissue. We point out here that the signs were modified from the original implementation of Chan and Vese[6], as we considered $\phi < 0$ inside the object to be consistent with the standard level set implementation. The spatial derivatives were computed with $\Delta x = \Delta y = \Delta z = 1$. The time step was set to $\Delta t = 100$ providing a fast evolution with stable behavior. No reinitialization of the level set function was used as the definition of the Heaviside and Dirac functions as non-zero over the entire domain ensured a global deformation of the curve. The zero level of the function might split into two close curves for data sets that include the two ventricles. The algorithm selected only the close surface that contains our initial points.

2.5. Convergence Criteria

In our previous implementation we did not have a convergence criteria and solely relied on a predefined number of iterations. The convergence criteria proposed by Chan and Vese, based on shape change around the level zero of the front did provide robust information in noisy cases with low contrast from the myocardium (where the front was moving slowly) or for cases with missing myocardium wall (where the front was leaking). We implemented in this work the dual convergence criteria proposed by Baillard and Barillot in [13], based on:

(1) The ratio of new voxels to the total number of voxels below a threshold set to -0.5. This measures the ratio of expansion of the curve in terms of inside voxels.
(2) The first derivative of the displacement function. In their work, Baillard and Barillot used the average

value of a stopping function derived from a posteriory proability of a transition at the interface. In our work, we simply computed the first derivative of the level set function at the interface, defined for absolute values of the Heaviside function above 0.5.

In their work, the authors proposed pre-defined threshold values for these two measures, based on empirical experiments. We initially followed the same approach but found that threshold values defined on RT3D data sets did not work on higher contrast Live3D data. On the other hand, for both data types, the two measures showed a bell curve behavior with a rising phase initially and then a fast decrease towards the initial level. From these observations, we decided to use the initial value (after one iteration) as the threshold level, leading to very robust behavior. Because of the diversity of data quality and contrast with both ultrasound machines, we still had to rely on a maximum number of iterations for some cases which was set to 10 iterations for RT3D and 5 iterations for Live3D data.

2.6. Smoothness Constraints

Experiments with our previous segmentation methods presented in [14] for a preliminary study on wall motion deformation and in [12] for assessment of the level set segmentation framework with a clinical study on patients with primary hypertension (PH), revealed significant issues on the smoothness of the shape and the importance of defining an accurate apex even though the ultrasound data is typically cropped and very noisy at this location. To handle these issues, recent work has focused on the introduction of shape priors in the level set energy functional such as in [15]. In our group we have tried to avoid this approach as shape models typically fail for abnormal wall motion cases and disease states as we observed for PH patients with very deformed right and left ventricles. In this work we have used constraints on the regularizing terms as described in the previous section, where we constrained the model to deform over only 3 iterations at the apex location over three slices and we used a post-processing of the binary segmented data with 3D spline fitting in spherical coordinates with 4 nodes in both angular values (i.e. 16 nodes). This approach has enabled us to resolve the bumpiness of our initial segmented volumes and full definition of the ventricular shapes from base to apex.

3. RESULTS

3.1. Experimental Setup

We acquired two data sets from healthy volunteers screened with both real-time three dimensional machines: Volumetrics (RT3D) and Sonos 7500 (Live3d) from Philips. Manual tracing was performed on the Live3d machine by a cardiac fellow. Segmentation was run with the 3D level set algorithm on denoised data after spatio-temporal brushlet expansion [16]. Initialization was performed by selecting center points at the apex and base locations. A cylinder was created from this center points with a radius set to 3 pixels. The RT3D data sets were segmented at a voxel resolution of [1.2mm 1.2mm 2.4mm] for [*x y z*]. Segmentation of Live3d data was performed at a resolution of [1.5mm 1.6mm 3.6mm] and [1.7mm 1.7mm 3.8mm] for [*x y z*].

3.2. Ventricular Shapes

We first looked at left ventricular geometries from the different methods at end-diastole (ED) and end-systole (ES). Results are illustrated in Figure 1 and Figure 2 after spline interpolation.

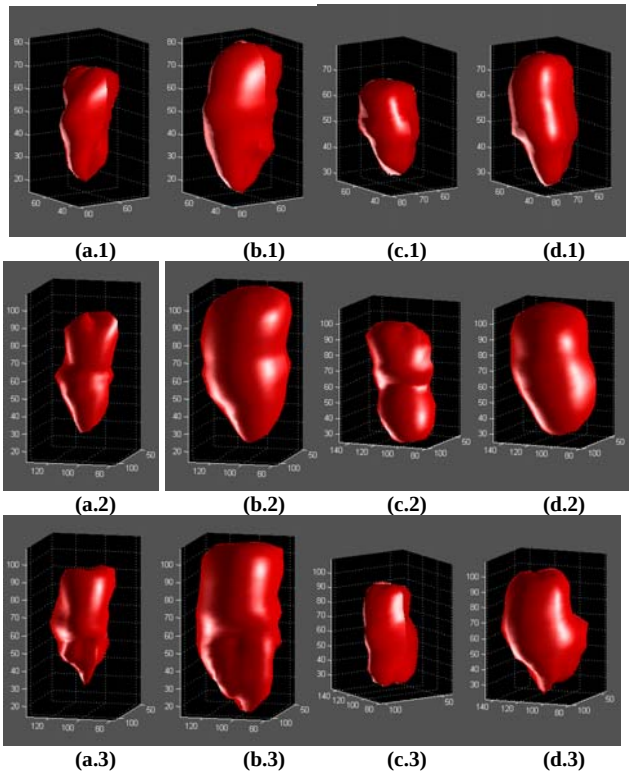

Figure 1: (a1~d1) Segmentation of RT3D data with 3D level set (LS3D). (a2~d2) Segmentation of Live3D data by manual tracing. (a3~d3) Segmentation of Live3D data with 3D level set. Volunteer #1: (a.1~a.3) ES, (b.1~b.3) ED. Volunteer #2: (c.1~c.3) ES, (d.1~d.3) ED.

Views from the two machines were rescaled to a common voxel size and manually co-registered for visualization. A precise registration should be incorporated for direct surface comparison.

3.2.1. Quantification of Ventricular Volumes

We present below the overlap of our segmentation methods of long axis views from a volunteer for manual and level set segmentation for a single volunteer with both ultrasound machines. The general overlap of both methods was quite significant defining a similar overall shape. Quantification of shape similarity is currently

being under investigation in collaboration with the cardiac mechanics laboratory to parameterize shape geometry through finite element modeling. A first study with our initial level set segmentation method showed the limitation of our method to carry out this modelization with non-smoothed data.

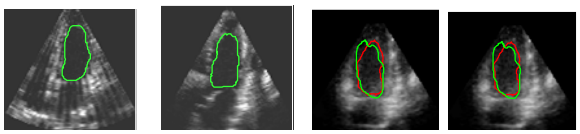

(a) (b) (c) (d)

Figure 2: Orthogonal long-axis slices from (a-b) RT3D data with LS3D contour; (c-d) Live3D data with manual tracing (red) and LS3D (green) contours.

We provide below a table summarizing ejection fraction (EF) measurements for the two volunteers on both RT3D and Live3D data. Previous clinical studies from our group have validated the use of disk summation on RT3D data for volume and EF measurement and we report these measurements, performed by a second clinical expert.

EF (%)	RT3D Disk	RT3D LS3D	Live3D Manual	Live3D LS3D
# 1	58.4	46.1	45.0	46.7
# 2	68.9	58.6	68.7	71.2

Table 1: Measurements of EF for the two volunteer cases.

Quantitative measurements revealed good agreement between LS3D and manual measurements by experts. Comparing the two ultrasound machines, we observed systematic larger volume measurements with Live3D than with RT3D but similar EF values.

4. CONCLUSION

Results presented in this paper showed encouraging results on the use of a homogeneity-based level set segmentation for real-time three-dimensional ultrasound data applied to two ultrasound machines. Quantification of cardiac function and visual comparison of ventricular shape showed strong similarities between the two 3D ultrasound machines and between the LS3D method and manual tracing by an expert. We have derived a robust segmentation method to handle the variety of data quality encountered in typical clinical screening of humans affected by both a patient's acoustic window and the ventricle size and shape.

The proposed method does not use prior shape models to constraint the level set deformations. While this approach offers greater flexibility in applying the segmentation to disease cases, it still faces problematic situations where data quality is very poor (such as in post-exercise stress echo data), or where cropping of the apex occurred. We are currently investigating better initialization methods to improve robustness of the method. Once fully validated, our segmentation method will be used to feed a ventricular mechanical model to quantity and parameterized endocardial wall deformation using the method introduced in [14]. A robust and flexible segmentation method is essential for the use of such models, which will help us understand better the accuracy of motion information that can be extracted from noisy echocardiographic data.

5. REFERENCES

[1] O. T. Von Ramm and S. W. Smith, "Real time volumetric ultrasound imaging system," *Journal of Digital Imaging*, vol. 3, pp. 261-266, 1990.

[2] J. A. Sethian, "Theory, algorithms , and applications of level set methods for propagating surfaces," *Acta Numerica*, pp. 309-395, 1996.

[3] W. J. Niessen, B. M. t. H. Romeny, and M. A. Viergever, "Geodesic deformable models for medical image analysis," *IEEE Transactions on Medical Imaging*, vol. 17, pp. 634 - 641, 1998.

[4] J. Montagnat, H. Delingette, and N. Ayache, "A review of deformable surfaces: topology, geometry and deformation," *Image and Vision Computing*, vol. 19, pp. 1023-1040, 2001.

[5] C. Xu, D. L. Pham, and J. L. Prince, "Image segmentation using deformable models," in *Handbook of Medical Imaging, Vol. 2: Medical Image Processing and Analysis*, vol. 2: SPIE Press, 2000, pp. 131-169.

[6] T. F. Chan and L. A. Vese, "Active contours without edges," *IEEE Transactions on Image Processing*, vol. 10, pp. 266 - 277, 2001.

[7] D. Mumford and J. Shah, "Boundary detection by minimizing functional," International Conference on Computer Vision and Pattern Recognition, San Francisco, CA, USA, pp. 22-26, 1985.

[8] S. Osher and J. A. Sethian, "Fronts propagating with curvature-dependent speed: Algorithms based on Hamilton-Jacobi formulations," *Journal of Computational Physics*, vol. 79, pp. 12-49, 1988.

[9] H.-K. Zhao, T. Chan, B. Merriman, and S. Osher, "A variational level set approach to multiphase motion," *Journal of computational physics*, vol. 127, pp. 179-195, 1996.

[10] L. I. Rudin, S. Osher, and E. Fatemi, "Nonlinear total variation based noise removal algorithms," *Physica D*, vol. 60, pp. 259--268, 1992.

[11] G. Aubert and L. Vese, "A variational method in image recovery," *SIAM Journal on Numerical Analysis*, vol. 34, pp. 1948-1979, 1997.

[12] E. D. Angelini, J. Holmes, A. F. Laine, and S. Homma, "Segmentation of real-time 3D cardiac ultrasound with implicit deformable models without gradients," International Symposium on Image and Signal Processing and Analysis, Rome, Italy, pp. 711-716, 2003.

[13] C. Baillard and C. Barillot., "Robust 3D segmentation of anatomical structures with level sets," MICCAI, Pittsburgh, PA, USA, pp. 236-245, 2000.

[14] E. D. Angelini, D. Hamming, S. Homma, J. Holmes, and A. Laine, "Comparison of segmentation methods for analysis of endocardial wall motion with real-time three-dimensional ultrasound," Computers in Cardiology, Memphis TN, USA, pp. 609-612, 2002.

[15] N. Paragios, "A level set approach for shape-driven segmentation and tracking of the left ventricle," *IEEE Transactions on Medical Imaging*, vol. 22, pp. 773 -776, 2003.

[16] E. Angelini, A. Laine, S. Takuma, J. Holmes, and S. Homma, "LV volume quantification via spatio-temporal analysis of real-time 3D echocardiography," *IEEE Transactions on Medical Imaging*, vol. 20, pp. 457-469, 2001.